Spectroscopy of the $^2S_{1/2} \rightarrow {}^2P_{3/2}$ transition in Yb II: Isotope shifts, hyperfine splitting, and branching ratios

T. Feldker, H. Fürst, N. V. Ewald, J. Joger, and R. Gerritsma

Van der Waals-Zeeman Institute, Institute of Physics (IoP), University of Amsterdam, Science Park 904, 1098 XH Amsterdam, The Netherlands

We report on spectroscopic results on the $^2S_{1/2} \rightarrow {}^2P_{3/2}$ transition in single trapped Yb$^+$ ions. We measure the isotope shifts for all stable Yb$^+$ isotopes except ^{173}Yb$^+$, as well as the hyperfine splitting of the $^2P_{3/2}$ state in ^{171}Yb$^+$. Our results are in agreement with previous measurements but are a factor of 5–9 more precise. For the hyperfine constant $A(^2P_{3/2}) = 875.4(10)$ MHz our results also agree with previous measurements but deviate significantly from theoretical predictions. We present experimental results on the branching ratios for the decay of the $^2P_{3/2}$ state. We find branching fractions for the decay to the $^2D_{3/2}$ state and $^2D_{5/2}$ state of 0.17(1)% and 1.08(5)%, respectively, in rough agreement with theoretical predictions. Furthermore, we measured the isotope shifts of the $^2F_{7/2} \rightarrow {}^1D[5/2]_{5/2}$ transition and determine the hyperfine structure constant for the $^1D[5/2]_{5/2}$ state in ^{171}Yb$^+$ to be $A(^1D[5/2]_{5/2}) = -107(6)$ MHz.

I. INTRODUCTION

Laser-cooled ions in Paul traps form one of the most mature laboratory systems for performing optical metrology, precision measurements, as well as quantum computation and quantum simulation [1–5]. The ion species Yb$^+$ is a particularly versatile system for many of these applications owing to its rich electronic structure with multiple metastable states [6,7]. Furthermore, the hyperfine structure of ^{171}Yb$^+$ provides a first-order magnetic-field-insensitive qubit in the electronic ground state [8–10] that may be used in quantum information applications [11,12].

While many transitions between low-lying electronic states in Yb$^+$ have been studied with great precision [10,13–17], there has been only one measurement of the isotope shifts in the $^2S_{1/2} \rightarrow {}^2P_{3/2}$ (D2) transition as well as of the hyperfine splitting of the $^2P_{3/2}$ state [18] so far, which was performed in a hollow-cathode discharge lamp. Remarkably, the experimental result for the hyperfine splitting disagrees significantly with theoretical predictions [19–23]. Although there has been a lot of theoretical work on transition amplitudes for the decay of the $^2P_{3/2}$ state [20–22,24,25], there seems to be no experimental data available for the branching ratios of the decay of the $^2P_{3/2}$ state up until now.

Here, we present experimental results on the isotope shifts in the D2 transition, the hyperfine splitting of the $^2P_{3/2}$ state, as well as on the branching ratios of its decay obtained from a single trapped and laser-cooled ion. Furthermore, we present measurements of the isotope shift in the $^2F_{7/2} \rightarrow {}^1D[5/2]_{5/2}$ transition, as well as the hyperfine splitting in the $^1D[5/2]_{5/2}$ state in ^{171}Yb$^+$. Single trapped ions are very well suited to perform such precision measurements, because both state preparation and detection can be performed with great accuracy while at the same time errors due to background gas collisions are negligible. Using isotope-selective photoionization to load the Paul trap, we are able to conduct the experiments even with the rare isotope ^{168}Yb$^+$

(0.13% abundance [26]), for which no previous data seem to exist.

II. EXPERIMENTAL SETUP

The experiments were performed in a linear Paul trap as described in Ref. [27]. We load a single Yb$^+$ ion into the trap by two-step photoionization with lasers at 399 nm wavelength for the resonant excitation of the $^1S_0 \rightarrow {}^1P_1$ transition in neutral Yb and 369 nm wavelength for the excitation into the ionization continuum. Tuning the wavelength of the first step to the resonance of a specific isotope allows for isotope-selective loading of Yb$^+$ ions. Due to overlapping resonances [28], ^{170}Yb$^+$ and ^{172}Yb$^+$ cannot be loaded deterministically, but only in combination with ^{171}Yb$^+$ and ^{173}Yb$^+$, respectively. However, by temporarily lowering the trap drive amplitude we can expel the heavier isotopes from the trap and keep only the isotope ^{170}Yb$^+$ or ^{172}Yb$^+$, respectively.

Lasers near wavelengths of 369 and 935 nm are used to Doppler cool the ion on the $^2S_{1/2} \rightarrow {}^2P_{1/2}$ transition and pump population trapped in the metastable $^2D_{3/2}$ state back into the cooling cycle via excitation to the $^3D[3/2]_{1/2}$ state, as shown in Fig. 1(a). We image the ion's fluorescence at 369 nm wavelength to a photomultiplier tube (PMT) for detection.

For cooling of the isotope ^{171}Yb$^+$, which has a nuclear spin of $I = 1/2$ and accordingly hyperfine splittings of the electronic states, we use the closed transition $|^2S_{1/2}, F = 1\rangle \rightarrow |^2P_{1/2}, F = 0\rangle$. However, due to off-resonant excitation of the $|^2P_{1/2}, F = 1\rangle$ state, the ion occasionally decays to the $|^2S_{1/2}, F = 0\rangle$ state. Microwave radiation at 12.6 GHz couples the $F = 0$ and $F = 1$ ground states to ensure continuous cooling. To prepare the ion in the $|^2S_{1/2}, F = 0\rangle$ state, we excite the $|^2S_{1/2}, F = 1\rangle \rightarrow |^2P_{1/2}, F = 1\rangle$ transition resonantly while the microwave radiation is switched off.

In addition to the lasers required for cooling and detection of the ion, we use light near the wavelengths of 329 and 638 nm
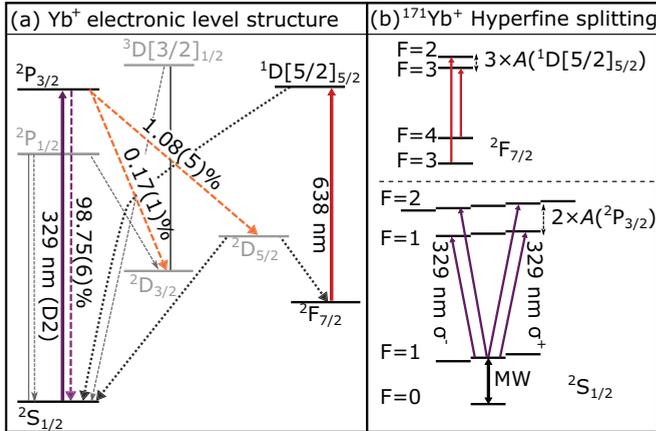
FIG. 1. (a) Relevant electronic levels and transitions in Yb$^+$. We perform spectroscopic measurements on the $^2S_{1/2} \to {}^2P_{3/2}$ ($D2$) transition near 329 nm wavelength. The $^2P_{3/2}$ state decays in $\tau = 6.15(9)$ ns [29] either back to the ground state or to one of the metastable states $^2D_{3/2}$ or $^2D_{5/2}$. While an ion which is initially in the state $^2S_{1/2}$ or $^2D_{3/2}$ scatters light during Doppler cooling (thin gray arrows), it will not scatter light when it is in the $^2D_{5/2}$ state. This allows for detection of a successful excitation of the $^2S_{1/2} \to {}^2P_{3/2}$ transition as well as for measurement of the branching fractions of the $^2P_{3/2}$ decay. From the $^2D_{5/2}$ state the ion decays in $\tau = 7.2(3)$ ms [13] to either the ground state or the very long lived $^2F_{7/2}$ state ($\tau \approx 10$ yr [30]). We use the $^2F_{7/2} \to {}^1D[5/2]_{5/2}$ transition near 638 nm wavelength to depopulate the $^2F_{7/2}$ state. (b) Hyperfine structure of the $^2F_{7/2} \to {}^1D[5/2]_{5/2}$ and $^2S_{1/2} \to {}^2P_{3/2}$ transitions in ^{171}Yb$^+$.

to drive the transitions $^2S_{1/2} \to {}^2P_{3/2}$ and $^2F_{7/2} \to {}^1D[5/2]_{5/2}$, respectively. We generate light at 329 nm wavelength with a frequency-quadrupled, amplified diode laser. After the first doubling cavity, light at 658 nm wavelength is coupled into a high-bandwidth fiber electro-optic modulator (EOM). Sidebands at frequencies of 0.1–3 GHz are modulated onto the light and used to stabilize the laser to an external reference cavity. Thus, the laser is stabilized to the fixed reference cavity with a variable frequency offset which is given by the modulation frequency of the EOM. The reference cavity consists of two mirrors with a reflectivity of $R \approx 99\%$ glued to a 10-cm-long Zerodur spacer in a temperature-stabilized vacuum housing. The laser is frequency stabilized by using the Pound–Drever–Hall technique [31].

For further frequency scanning and pulse shaping we use an acousto-optic modulator (AOM) in double-pass configuration with a center frequency of 200 MHz and a bandwidth of 100 MHz. The signals for the AOM and the fiber EOM are generated by a two-channel microwave generator, which is stabilized to a 10 MHz reference signal from a signal generator. A mechanical shutter prevents any light from reaching the ion if switched off. Light from the first doubling cavity is coupled to a commercial wavelength meter, allowing for a coarse absolute frequency determination of the frequency-quadrupled light with an accuracy of 60 MHz according to specification.

We generate light at 638 nm wavelength with a home-made ECDL. This laser is stabilized to the wavelength meter to compensate for frequency drifts and has a short-time frequency stability of better than 10 MHz. We switch the light with a
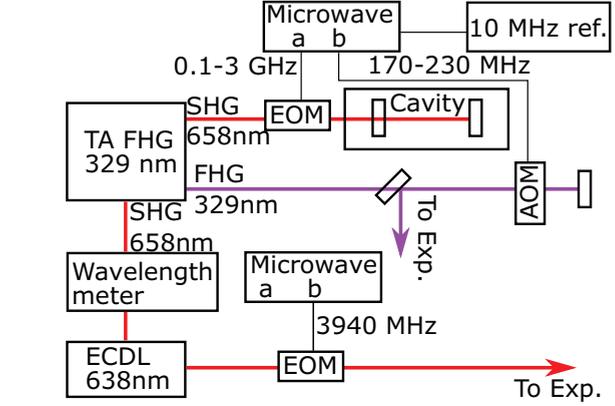
FIG. 2. Sketch of laser setup for excitation of the $^2F_{7/2} \to {}^1D[5/2]_{5/2}$ and $^2S_{1/2} \to {}^2P_{3/2}$ transitions. Radiation near 329 nm wavelength is generated by a frequency-quadrupled, amplified diode laser. After the first frequency doubling, part of the light is coupled out and used for frequency stabilization to a fixed reference cavity. By using a fiber-coupled electro-optic modulator (EOM), we generate sidebands with a frequency between 0.1–3 GHz which are used to offset the laser's carrier frequency with respect to the cavity mode. We use an acousto-optic modulator (AOM) in double-pass configuration for pulse shaping and frequency scanning. The laser at 638 nm wavelength is a home-made external-cavity diode laser (ECDL) with a grating in Littrow configuration. It is frequency stabilized to the wavelength meter and switched by a mechanical shutter. Using a fiber EOM, sidebands can be modulated in order to drive transitions between multiple hyperfine states.

mechanical shutter. The light is coupled to a fiber EOM, which allows for modulating sidebands in order to drive transitions between multiple hyperfine states in the case of ^{171}Yb$^+$, and guided to the experiment. The part of the setup relevant for the spectroscopy is shown in Fig. 2.

III. RESULTS

A. Isotope shifts and hyperfine splitting

In the case of isotopes without nuclear spin, we measure the resonance frequency of the $D2$ transition by applying laser pulses with a width of 5 μs and a saturation parameter $s \approx 1$ to the ion. From the $^2P_{3/2}$ state, there is a probability of about 1% for the ion to decay to the metastable state $^2D_{5/2}$ ($\tau = 7.2$ ms) from where it decays with 83% probability [13] to the long-lived $^2F_{7/2}$ state. An ion in either of these states does not scatter light during Doppler cooling. On resonance, about 50% of the population decays to the dark $^2D_{5/2}$ state in 5 μs. To detect whether the ion is in one of the dark states, we image the ion's fluorescence to a PMT for 4 ms during Doppler cooling, allowing for almost-perfect state detection. We scan the laser over the atomic resonance in steps of 2 MHz by tuning the drive frequency of the AOM (ν_{aom}). We compensate for the frequency dependence of the diffraction efficiency in the AOM by supplying appropriate radio-frequency power at each frequency. After the detection, we pump the ion back into the cooling cycle by exciting the $^2F_{7/2} \to {}^1D[5/2]_{5/2}$ transition. A postselection measurement is performed before each spectroscopy pulse in order to check if the ion was successfully
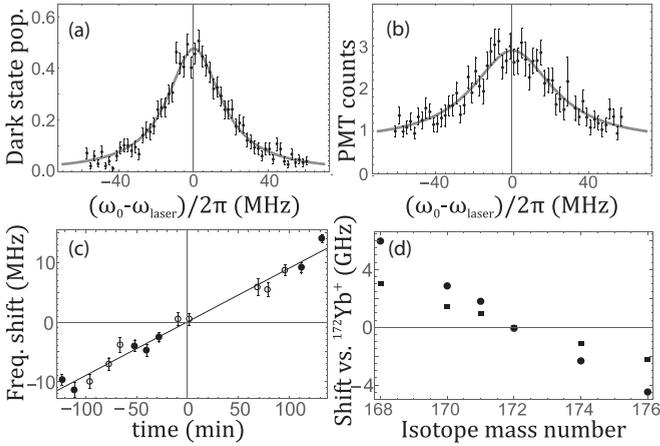
FIG. 3. Isotope-shift measurement with trapped Yb$^+$ ions. (a) Data from a single scan over the $^2S_{1/2} \rightarrow {}^2P_{3/2}$ transition in ^{174}Yb$^+$. Error bars denote the quantum projection noise. (b) Plot of a single resonance scan in ^{171}Yb$^+$. Here, we do not project to bright or dark states but measure PMT counts during the detection bin ($t_{\text{det}} = 2.5$ ms). The error bars denote the uncertainties from photon counting statistics. (c) Cavity drift obtained by repeated measurements of the transitions from $|^2S_{1/2}, F = 1\rangle$ to $|^2P_{3/2}, F = 1\rangle$ (circles) or $|^2P_{3/2}, F = 2\rangle$ (disks). Offsets of $\nu_1 = 1811.0$ MHz ($F = 1$, circles) and $\nu_2 = -60.0$ MHz ($F = 2$, disks) are added to the measured resonance frequencies. We choose ν_1 and ν_2 so that the standard deviation for a combined linear fit (black line) is minimized. From the gradient of the fit, we determine a linear drift of the cavity of 92 kHz/min. The hyperfine splitting of the $^2P_{3/2}$ state is given by the difference $\nu_1 - \nu_2 = 1751.0$ MHz. The result given in Table II is based on the average of two measurement series on different days. (d) Isotope shifts in the $^2S_{1/2} \rightarrow {}^2P_{3/2}$ transition (circles) and the $^2F_{7/2} \rightarrow {}^1D[5/2]_{5/2}$ transition (squares). Error bars are too small to be visible on this scale.

pumped out of the $^2F_{7/2}$ state. The measurement data for a single scan of the transition in ^{174}Yb$^+$ are plotted in Fig. 3(a).

We repeat the experiment for the isotopes ^{168}Yb$^+$, ^{170}Yb$^+$, ^{172}Yb$^+$, ^{174}Yb$^+$, and ^{176}Yb$^+$. For each measurement, we frequency stabilize the laser to the same cavity mode, but with different offset frequencies ν_{eom} given by the modulation frequency of the fiber EOM. The relative frequency of the spectroscopy light compared with the fixed cavity resonance is determined by $\nu_{\text{rel}} = 2\nu_{\text{eom}} - 2\nu_{\text{aom}}$. We estimate the drift of the cavity by measuring the same resonance at different times as shown in Fig. 3(c).

We determine the resonance frequencies by fitting a Lorentzian lineshape to the measured data. The uncertainties in the energy shifts are dominated by the standard error of the least-squares fit (0.5–1 MHz) and the uncertainty in the cavity drift during the measurement time of a few hours. In principle, the error should not depend on the abundance of the isotope. However, the measurements with the rare isotopes ^{168}Yb$^+$ (0.13% abundance) and ^{170}Yb$^+$ (3.05% abundance, can only be loaded in combination with ^{171}Yb$^+$) [26] take significantly longer due to low ion-loading rates. This leads to larger uncertainties for the cavity drift of about 3 MHz, compared with 1 MHz for the more abundant isotopes ^{172}Yb$^+$, ^{174}Yb$^+$, and ^{176}Yb$^+$. We use π-polarized light and a small magnetic field of $B = 0.05$ mT to avoid errors due to Zeeman shifts of the $D2$ transition. The results shown in Fig. 3(d) and Table I are based on the average of two measurement series on different days. The difference between these datasets is in agreement with the quoted uncertainties.

In the case of ^{171}Yb$^+$ we make use of the hyperfine structure [see Fig. 1(b)] in order to detect the excitation to the $^2P_{3/2}$ state. We prepare the ion in the $|F = 0\rangle$ ground state before transferring it to the $|F = 1, m_F = 0\rangle$ state via rapid adiabatic passage (RAP) using microwave radiation. We apply a laser pulse with a width of 200 ns to excite the $|^2P_{3/2}, F = 1\rangle$ or $|^2P_{3/2}, F = 2\rangle$ states, followed by a second RAP pulse on the $|F = 0\rangle \rightarrow |F = 1, m_F = 0\rangle$ transition. At the end of this sequence, we perform state-selective fluorescence detection based on Doppler cooling without microwave coupling of the $|F = 1\rangle$ and $|F = 0\rangle$ ground states. During the detection, an ion in the $|F = 0\rangle$ state appears dark while an ion in the $|F = 1\rangle$ state scatters light, which allows for detection of the induced population transfer out of the initial $|F = 1, m_F = 0\rangle$ state.

Experiments with ^{171}Yb$^+$ are conducted in a magnetic field of 0.18–0.23 mT in order to allow for efficient Doppler cooling on the $|^2S_{1/2}, F = 1\rangle \rightarrow |^2P_{1/2}, F = 0\rangle$ transition [10]. We use linearly polarized light ($\sigma^+ + \sigma^-$) at 329 nm wavelength to avoid the dipole-forbidden $|^2S_{1/2}, F = 1, m_F = 0\rangle \rightarrow |^2P_{3/2}, F = 1, m_F = 0\rangle$ transition. Due to the symmetric excitzation of the transition [see Fig. 1(b)] the magnetic field should not lead to a frequency shift of the transition. Measurements at different fields corroborate this assumption.

We repeat the experiment for both hyperfine states and determine the hyperfine energy splitting given in Table II. We compare the transition frequencies to the resonance frequency for the isotope ^{172}Yb$^+$. Together with the well-known energy splitting of the ground state of 12642.812 MHz [9] we calculate

TABLE I. Isotope shifts of the $^2P_{3/2}$ state in Yb$^+$ as measured by our group compared with values from Ref. [18]. The number in brackets denotes the error in the last digit. The isotope shift of the $^2F_{7/2} \rightarrow {}^1D[5/2]_{5/2}$ transition as measured with the wavelength meter is given in the last column.

Yb$^+$ isotope	$^2P_{3/2}$ (this work)	$^2P_{3/2}$ (Ref. [18])	$^2F_{7/2} \rightarrow {}^1D[5/2]_{5/2}$ (this work)
168	3007.8(30) MHz		6.04(2) GHz
170	1457.9(30) MHz	1459(21) MHz	2.93(2) GHz
171	922.5(25) MHz	920(15) MHz	1.87(2) GHz
172	0	0	0
174	−1152.3(15) MHz	−1154(11) MHz	−2.26(2) GHz
176	−2254.8(15) MHz	−2259(13) MHz	−4.41(2) GHz

TABLE II. Hyperfine structure constants A in ^{171}Yb$^+$ in MHz. The number in brackets denotes the error in the last digit. The magnetic-dipole hyperfine-structure constant $A(^2P_{3/2})$ measured by our group is consistent with previous measurements (Expt) but deviates significantly from theory (Theor) predictions. In Ref. [21] results are given for a single-electron approach (a) and a many-electron approach (b). The many-electron results give by far the best agreement with our experimental results.

	[19]$_{\text{Theor}}$	[20]$_{\text{Theor}}$	[21]$^a_{\text{Theor}}$	[21]$^b_{\text{Theor}}$	[22]$_{\text{Theor}}$	[23]$_{\text{Theor}}$	[18]$_{\text{Expt}}$	This work
$A(^2P_{3/2})$	391	311.5	330	765	322	388	877(16)	875.4(10)
$A(^1D[5/2]_{5/2})$								$-107(6)$

the isotope shift of the $^2P_{3/2}$ state given in Table I. The uncertainty of 2.5 MHz for the isotope shift is again dominated by the error of the least-squares fit of the resonances (1 MHz) and the uncertainty of the cavity drift during the measurement time. For the uncertainty of the hyperfine constant, the cavity drift is less significant because we do not switch between isotopes during the experiment and thus are able to quickly switch between the measurement of the two hyperfine states.

During the spectroscopy of the $^2S_{1/2} \rightarrow {}^2P_{3/2}$ transition, the $^2F_{7/2}$ state with a lifetime of $\tau > 10$ yr [30] is populated via decay of the $^2D_{5/2}$ state. After the state detection, we pump population out of the $^2F_{7/2}$ state by excitation of the $^2F_{7/2} \rightarrow {}^1D[5/2]_{5/2}$ transition. We stabilize the laser to a wavelength meter, which yields a laser linewidth of better than 10 MHz. Efficient pumping out of the $^2F_{7/2}$ state is achieved in a frequency range of about ± 5 MHz around the chosen lock point. The estimated uncertainty of 20 MHz consists predominantly of the laser linewidth and the uncertainty of the lock point. We only rely on the relative accuracy of the wavelength meter in a very small frequency range of a few GHz. We are confident that this relative accuracy is much better than the absolute accuracy of the wavelength meter which is specified to be 30 MHz. Comparison of the $5s^2\,{}^1S_0 \rightarrow 5s5p\,{}^3P_1$ transition in ^{88}Sr at 434.829121 THz [32], which we use for calibration to the nearby $D2$ line in ^{6}Li at 446.799574 THz [33], corroborates this assumption.

To the best of our knowledge, this is the most complete (in terms of measured isotopes) and precise measurement of the isotope shifts of the $^2F_{7/2} \rightarrow {}^1D[5/2]_{5/2}$ transition. In ^{171}Yb$^+$ we drive the transitions $|F = 4\rangle \rightarrow |F = 3\rangle$ and $|F = 3\rangle \rightarrow |F = 2\rangle$ [see Fig. 1(b)]. We use sidebands at 3940 MHz to excite both transitions efficiently. We find that efficient pumping is achieved in a frequency range of 3930–3950 MHz. With a hyperfine splitting of the $^2F_{7/2}$ state of 3620(2) MHz [14], we determine an energy splitting of the upper $^1D[5/2]_{5/2}$ state of 320(20) MHz and a hyperfine constant $A(^1D[5/2]_{5/2}) = -107(6)$ MHz. There seems to be no previous experimental data available for the $^1D[5/2]_{5/2}$ hyperfine splitting, only a theoretical estimate of $A = 199$ MHz [34], which deviates significantly from the value we find in the experiment.

B. Branching fractions

To measure the branching fractions for decay out of the $^2P_{3/2}$ state, we excite the $D2$ transition with a short pulse of resonant light, followed by fluorescence detection of 100 μs duration. From the excited $^2P_{3/2}$ state, the ion decays either back to the ground state from where it may be excited to the $^2P_{3/2}$ state again, or to one of the metastable ^2D states.

During the subsequent fluorescence detection, an ion initially in the $^2S_{1/2}$ or $^2D_{3/2}$ state scatters light, while an ion in the $^2D_{5/2}$ state appears dark. By applying a pulse of light resonant with the $D2$ transition we transfer the population from the initial (bright) $^2S_{1/2}$ to a mixed state of $^2D_{3/2}$ (bright) and $^2D_{5/2}$ (dark). As a result, the photon-scattering rate $\nu_{\text{Ph}}(t_{329} = \infty)$ is only a fraction of the initial rate given by

$$\nu_{\text{Ph}}(t_{329} = \infty) = \nu_{\text{Ph}}(t_{329} = 0) \frac{f(D_{3/2})}{f(D_{3/2}) + f(D_{5/2})}, \quad (1)$$

where $f(D_{3/2})$ and $f(D_{5/2})$ are the branching fractions into the $^2D_{3/2}$ state and $^2D_{5/2}$ state, respectively.

Scanning the width of the resonant excitation pulse, we obtain the PMT counts versus pulse width plotted in Fig. 4. A least-squares fit of an exponential decay to the data yields a time constant $\tau_{\text{dark}} = 1.04(4)$ μs for the transfer from the initial bright $^2S_{1/2}$ state, to the mixed ^2D state with reduced fluorescence.

From the time constant τ_{dark} obtained by the fit, the lifetime of the $^2P_{3/2}$ state of $\tau_{p32} = 6.15(9)$ ns [29] and the probability to be in the excited state during the laser pulse $p_{p32} = 0.48(1)$, we determine the combined branching ratio to both ^2D states as follows:

$$p(^2D) = \frac{\tau_{p32}}{p_{p32}\tau_{\text{dark}}}. \quad (2)$$

Additionally, we obtain the ratio of the fluorescence at $t_{329} = \infty$ to the initial fluorescence at $t_{329} = 0$ from the measured data as $\nu_{\text{Ph}}(t_{329} = \infty) = 0.104(5)$ to $\nu_{\text{Ph}}(t_{329} = 0) = 0.74(2)$. According to Eq. (1), this corresponds to $f(D_{3/2})/f(D_{5/2}) = 0.16(1)$. Combining this with the result from Eq. (2), we determine branching fractions to the $^2D_{5/2}$ state and $^2D_{3/2}$ state of 1.08(5)% and 0.17(1)%, respectively,

TABLE III. Branching fractions of the decay from the $^2P_{3/2}$ state: Our work and the theoretical (Theor) predictions. In Ref. [21], results from a single-electron approach (a) and a many-electron approach (b) are given. Our values agree roughly with theoretical predictions.

Branching from $^2P_{3/2}$ to	[24]$_{\text{Theor}}$	[21]$^a_{\text{Theor}}$	[21]$^b_{\text{Theor}}$	[22]$_{\text{Theor}}$	[25]$_{\text{Theor}}$	This work
$^2S_{1/2}$	98.77%	98.86%	99.09%	98.86%	98.83%	98.75(6)%
$^2D_{3/2}$	0.21%	0.18%	0.15%	0.18%	0.19%	0.17(1)%
$^2D_{5/2}$	1.02%	0.96%	0.76%	0.96%	0.98%	1.08(5)%

FIG. 4. Branching-ratio measurement of the $^2P_{3/2}$ state. Plot of PMT counts during a 100 μs detection bin versus pulse width of a laser pulse (t_{329}), resonant with the $D2$ transition (blue) and background counts measured without an ion in the trap during the same 100 μs detection bin (yellow). From the decay time constant τ_{dark} we determine the combined decay probability to the ^2D states. From the ratio of fluorescence levels $n(D_{5/2})/n(D_{3/2})$, we determine the relative strength of the decays to the ^2D manifold. The inset shows a scan over the $^2S_{1/2} \rightarrow {}^2P_{3/2}$ resonance at a saturation parameter of $s = 11$ (blue). For comparison, the calculated nonsaturated line is shown (yellow).

which is in agreement with theoretical predictions from Ref. [24] (see Table III). The errors include the statistical uncertainties in τ_{dark}, $\nu_{Ph}(t_{329} = 0)$, $\nu_{Ph}(t_{329} = \infty)$ as well as uncertainties in the excited-state population and the lifetime of the $^2P_{3/2}$ state.

The result is based on two independent measurements on different days. Fitting the individual results of these two measurements yields branching fractions to the $^2D_{5/2}$ state of 1.05(7)% and 1.10(7)% as well as branching fractions to the $^2D_{3/2}$ state of 0.17(1)% for both measurements, which is well within the given uncertainties. As an additional consistency check we perform fits of subsets of the data, using only the even (uneven) time bins. The results are in agreement with the quoted uncertainties.

The saturation parameter s and thus the excited-state population probability p_{p32} in Eq. (2) is determined by a frequency scan over the resonance. We normalize the power in the 329 nm beam during the scan by appropriate power settings of the AOM as described above. We choose a short pulse width of $t_{329} = 500$ ns to avoid saturation of the decay to the $^2D_{5/2}$ state. We measure a saturation parameter of $s = 11$; the data are shown in the inset of Fig. 4. For the branching-ratio experiment we tune the laser to resonance and operate the AOM at the frequency of maximum diffraction efficiency, which allows us to increase the power in the laser pulse by a factor of 2.2 compared with the scan. Accordingly, we calculate a saturation parameter of $s = 24(13)$ for the branching-ratio experiment,

corresponding to a probability of being in the excited state of $p_{p32} = 0.48(1)$. This scan is repeated frequently during the measurement to monitor intensity and frequency drifts.

The cumulative duration of the excitation pulse ($t_{329} < 12\,\mu$s) and the detection bin ($t_{det} = 100\,\mu$s) is small compared with the lifetimes of the $^2D_{3/2}$ ($\tau > 50$ ms [15,16]) and $^2D_{5/2}$ ($\tau = 7.2$ ms [13]) states. The probability of decay back to the ground state during that time is less than 0.3% and thus is negligible compared with other experimental errors.

IV. CONCLUSIONS

We report on spectroscopic results on the $^2S_{1/2} \rightarrow {}^2P_{3/2}$ transition in single trapped Yb$^+$ ions. We find the branching fractions for decay of the $^2P_{3/2}$ state to the $^2D_{5/2}$ state and $^2D_{3/2}$ states to be 1.08% and 0.17%, respectively, in rough agreement with theoretical predictions from single-electron methods.

The isotope shifts in the $^2S_{1/2} \rightarrow {}^2P_{3/2}$ transition in Yb$^+$ and hyperfine splitting (in ^{171}Yb$^+$) of the $^2P_{3/2}$ state have been determined. Our results on both agree with previous results from Ref. [18] but are more precise by a factor of 5–9. Our results contradict theoretical predictions obtained from single-valence-electron approaches for the hyperfine splitting by a factor of 2–3.

Calculations of the properties of electronic states in Yb$^+$ are complicated because energetically-low-lying states with electrons excited from the f shell can strongly interact with states with filled f shell. Including states with unfilled f shells in the calculations requires a many-electron approach [21]. However, the methods for many-electron calculations are generally less precise compared with single-valence-electron calculations. In particular, the $^2P_{3/2}$ state has a completely filled f shell but mixes strongly with the energetically close $^3[3/2]^o_{3/2}$ state of the $4f^{13}5d6s$ configuration. This mixing could explain the relatively large discrepancy between experiment and theory based on single-electron methods [21].

Indeed, the hyperfine constant calculated by a many-electron approach [21] agrees much better with our experimental result. However, the theoretical prediction obtained with the many-electron method still deviates from our experimental result by many standard deviations. Precise knowledge of properties of states with strong mixing to states with holes in the f shell such as the $^2P_{3/2}$ state measured in this work may thus serve as a test-bed for many-electron methods in Yb$^+$.

[1] S. A. Diddams, T. Udem, J. C. Bergquist, E. A. Curtis, R. E. Drullinger, L. Hollberg, W. M. Itano, W. D. Lee, C. W. Oates, K. R. Vogel, and D. J. Wineland, Science **293**, 825 (2001).

[2] N. Fortson, Phys. Rev. Lett. **70**, 2383 (1993).

[3] H. Häffner, T. Beier, N. Hermanspahn, H. J. Kluge, W. Quint, S. Stahl, J. Verdu, and G. Werth, Phys. Rev. Lett. **85**, 5308 (2000).

[4] J. I. Cirac and P. Zoller, Phys. Rev. Lett. **74**, 4091 (1995).

[5] R. Blatt and C. F. Roos, Nat. Phys. **8**, 277 (2012).

[6] C. Tamm, S. Weyers, B. Lipphardt, and E. Peik, Phys. Rev. A **80**, 043403 (2009).

[7] R. M. Godun, P. B. R. Nisbet-Jones, J. M. Jones, S. A. King, L. A. M. Johnson, H. S. Margolis, K. Szymaniec, S. N. Lea, K. Bongs, and P. Gill, Phys. Rev. Lett. **113**, 210801 (2014).

[8] R. Blatt, H. Schnatz, and G. Werth, Z. Phys. A: At. Nucl. (1975) **312**, 143 (1983).

[9] P. Phoonthong, M. Mizuno, K. Kido, and N. Shiga, Appl. Phys. B: Lasers Opt. **117**, 673 (2014).

[10] S. Olmschenk, K. C. Younge, D. L. Moehring, D. Matsukevich, P. Maunz, and C. Monroe, Phys. Rev. A **76**, 052314 (2007).

[11] R. Islam, C. Senko, W. C. Campbell, S. Korenblit, J. Smith, A. Lee, E. E. Edwards, C.-C. J. Wang, J. K. Freericks, and C. Monroe, Science **340**, 583 (2013).

[12] S. Debnath, N. M. Linke, C. Figgatt, K. A. Landsman, K. Wright, and C. Monroe, Nature (London) **536**, 63 (2016).

[13] P. Taylor, M. Roberts, S. V. Gateva-Kostova, R. B. M. Clarke, G. P. Barwood, W. R. C. Rowley, and P. Gill, Phys. Rev. A **56**, 2699 (1997).

[14] P. Taylor, M. Roberts, G. M. Macfarlane, G. P. Barwood, W. R. C. Rowley, and P. Gill, Phys. Rev. A **60**, 2829 (1999).

[15] N. Yu and L. Maleki, Phys. Rev. A **61**, 022507 (2000).

[16] M. Schacht, J. R. Danielson, S. Rahaman, J. R. Torgerson, J. Zhang, and M. M. Schauer, J. Phys. B: At., Mol. Opt. Phys. **48**, 065003 (2015).

[17] C. Tamm, B. Lipphardt, H. Schnatz, R. Wynands, S. Weyers, T. Schneider, and E. Peik, IEEE Trans. Instrum. Meas. **56**, 601 (2007).

[18] R. W. Berends and L. Maleki, J. Opt. Soc. Am. B **9**, 332 (1992).

[19] A.-M. Martensson-Pendrill, D. S. Gough, and P. Hannaford, Phys. Rev. A **49**, 3351 (1994).

[20] U. I. Safronova and M. S. Safronova, Phys. Rev. A **79**, 022512 (2009).

[21] S. G. Porsev, M. S. Safronova, and M. G. Kozlov, Phys. Rev. A **86**, 022504 (2012).

[22] B. K. Sahoo and B. P. Das, Phys. Rev. A **84**, 010502(R) (2011).

[23] V. A. Dzuba and V. V. Flambaum, Phys. Rev. A **83**, 052513 (2011).

[24] E. Biemont, J. F. Dutrieux, I. Martin, and P. Quinet, J. Phys. B: At., Mol. Opt. Phys. **31**, 3321 (1998).

[25] B. M. Roberts, V. A. Dzuba, and V. V. Flambaum, Phys. Rev. A **89**, 012502 (2014).

[26] NIST Atomic Spectra Database https://physics.nist.gov/.

[27] J. Joger, H. Fürst, N. Ewald, T. Feldker, M. Tomza, and R. Gerritsma, Phys. Rev. A **96**, 030703(R) (2017).

[28] M. Kleinert, M. E. Gold Dahl, and S. Bergeson, Phys. Rev. A **94**, 052511 (2016).

[29] E. H. Pinnington, G. Rieger, and J. A. Kernahan, Phys. Rev. A **56**, 2421 (1997).

[30] M. Roberts, P. Taylor, G. P. Barwood, P. Gill, H. A. Klein, and W. R. C. Rowley, Phys. Rev. Lett. **78**, 1876 (1997).

[31] R. W. P. Drever, J. L. Hall, F. V. Kowalski, J. Hough, G. M. Ford, A. J. Munley, and H. Ward, Appl. Phys. B: Photophys. Laser Chem. **31**, 97 (1983).

[32] G. Ferrari, P. Cancio, R. Drullinger, G. Giusfredi, N. Poli, M. Prevedelli, C. Toninelli, and G. M. Tino, Phys. Rev. Lett. **91**, 243002 (2003).

[33] C. J. Sansonetti, C. E. Simien, J. D. Gillaspy, J. N. Tan, S. M. Brewer, R. C. Brown, S. Wu, and J. V. Porto, Phys. Rev. Lett. **107**, 023001 (2011).

[34] M. J. Petrasiunas, E. W. Streed, T. J. Weinhold, B. G. Norton, and D. Kielpinski, Appl. Phys. B: Lasers Opt. **107**, 1053 (2012).